Aerosol Science and Technology

ISSN: 0278-6826 (Print) 1521-7388 (Online) Journal homepage: informahealthcare.com/journals/uast20

Generation of TiO_2 Aerosols from Liquid Suspensions: Influence of Colloid Characteristics

Virginia Gomez, Silvia Irusta, Francisco Balas & Jesus Santamaria

To cite this article: Virginia Gomez, Silvia Irusta, Francisco Balas & Jesus Santamaria (2013) Generation of TiO_2 Aerosols from Liquid Suspensions: Influence of Colloid Characteristics, Aerosol Science and Technology, 47:12, 1383-1392, DOI: 10.1080/02786826.2013.845645

To link to this article: https://doi.org/10.1080/02786826.2013.845645

Aerosol Science and Technology, 47:1383–1392, 2013

ISSN: 0278-6826 print / 1521-7388 online
DOI: 10.1080/02786826.2013.845645

Generation of TiO_2 Aerosols from Liquid Suspensions: Influence of Colloid Characteristics

Virginia Gomez,[1] Silvia Irusta,[1,2] Francisco Balas,[1,2,3] and Jesus Santamaria[1,2]

[1]*Aragon Institute of Nanoscience, University of Zaragoza, Zaragoza, Spain*
[2]*Networking Biomedical Research Centre of Biomaterials, Bioengineering and Nanomedicine, Zaragoza, Spain*
[3]*Instituto de Carboquímica, Consejo Superior de Investigaciones Científicas, Zaragoza, Spain*

The influence of the colloidal characteristics of aqueous TiO_2 nanoparticle suspensions and of the operating conditions on the total particle concentration and the particle size distribution of aerosols generated by nebulization has been studied. A commercial nebulization unit coupled to a diffusion dryer was used to generate aerosols using two different sources of titanium dioxide nanoparticles. Stable, concentration-tunable aerosols could be obtained for both types of nanoparticle suspensions. The effect of operating conditions during nebulization (air flow rate, purity of water source, nanoparticle concentration, and pH of the precursor suspension) was studied. The results obtained indicate that the degree of agglomeration in the liquid phase previous to aerosol formation has a direct influence both on the total nanoparticle count and on the particle size distribution of the generated aerosols.

[Supplementary materials are available for this article. Go to the publisher's online edition of *Aerosol Science and Technology* to view the free supplementary files.]

1. INTRODUCTION

Among the current technologies for producing aerosols, pneumatic nebulization of colloidal suspensions is one of the simplest and most convenient. These wet-phase generators provide a stable stream of aerosolized particles that can be used in a wide variety of applications from biomedicine (Henning et al. 2010) to synthetic chemistry (Kodas 1999). In a concise manner, a nebulizer is a device that uses a gas stream with a sufficiently high speed to break up a liquid into a cloud of small droplets. The mist obtained is formed by liquid drops containing the desired particles and is then subjected to drying. After evaporation of the liquid in each droplet, an aerosol stream is produced (Hinds 1999). Both droplet size distribution and concentration of liquid droplets in the aerosol depend on several parameters such as the gas pressure through the nebulizer, the properties of the liquid, and, ultimately, the design of the nebulizing nozzle (Swift 1993). On the other hand, the particle size distribution and the concentration of particles in the liquid suspension determine the characteristics of the aerosol obtained after the drying process.

In view of its relatively easy implementation, nebulization of colloidal suspensions of nanosized particles is one of the preferred methods to produce stable nanoparticle aerosol streams. In this way, nanoparticle suspensions with carefully tailored characteristics can be prepared and used as the precursor of the aerosol in a variety of applications. Thus for instance, this concept has been intensely studied in view of its implications on drug delivery using the upper respiratory ways (Yeo et al. 2010; Beck-Broichsitter et al. 2013; Verma et al. 2013). Also, given the possible health and environmental impacts of nanoparticles (Wiesner et al. 2006), nebulizer-generated nanoparticle aerosols with a wide range of aerodynamic sizes and mass concentrations are frequently used to test the efficiency of filters against nanoparticles (Eninger et al. 2009; Shimada et al. 2009) as well as for the development of deposition samplers (Cena et al. 2011). Inhaled nanoparticles not only may cause direct damage to lung tissue, but also are able to translocate from the respiratory ways to the bloodstream (Borm et al. 2002; Oberdörster et al. 2002, 2004). Harmful effects of the inhalation of nanoparticles have been reported, for example, for carbon nanotubes (Zhang et al. 2010), silicon dioxide (Napierska et al. 2010), or titanium dioxide nanoparticles (Rossi et al. 2010). Again in this

Received 20 June 2013; accepted 10 August 2013.

The authors would like to thank financial support through research projects Nanotrap (MAT2008-01319/NAN) and Nanosost (PSE-420000-2008-3) of the Spanish Ministry of Economy and Competitivity and NanoValid (Contract No. 263147) of the European Union FP7 Framework Programme. Francisco Balas would like to thank the "Ramon y Cajal" tenure grant (RYC-2011-07641) and Virginia Gomez would like to thank the FPU scholarship AP2008-02067.

Address correspondence to Francisco Balas or Jesus Santamaria, Aragon Institute of Nanoscience (INA), University of Zaragoza, c/Mariano Esquillor s/n, Zaragoza 50018, Spain. E-mail: fbalas@unizar.es; Jesus.Santamaria@unizar.es

case, nebulizer-generated aerosols are ideally suited for testing the health impact of nanoparticles. Thus for instance, McJilton et al. (2009) used pneumatic nebulization of carbon nanotubes in studies of respiratory toxicology.

The colloidal state of the suspensions prior to and during nebulization is of paramount importance to determine the aerosol characteristics. The influence of the agglomeration of colloidal particles in the size and concentration of nanosized TiO_2 particles upon nebulization (Noël et al. 2012) has been recently analyzed. The authors showed the importance of a qualitative and quantitative characterization of the nanoparticles and their agglomerates on the characteristics of the resulting aerosols. It has also been reported that the presence of residual content from the solvent either forms individual particles or become adhered to the particles in the colloid, effectively increasing the resulting particle sizes, and possibly changing the surface chemistry of airborne nanoparticles (Park et al. 2012). The surface charge of particles in the suspension may also influence aerosol generation, modifying the aggregation state of particles during the nebulization.

Therefore, there is a need to deeply examine the influence of the colloidal properties of nanoparticle suspensions on the final characteristics of aerosols generated through pneumatic nebulization. In this work, we study the colloidal suspensions produced with TiO_2 (anatase) nanoparticles obtained from different sources. First, commercial anatase nanoparticles were tested, together with synthetic TiO_2 nanoparticles obtained in our laboratory through a microwave-assisted method described elsewhere (Gomez et al. 2012). In this work, we have attempted a comprehensive study of the main variables influencing nanoparticle aerosol generation through nebulization of colloidal nanoparticle suspensions. We have also analyzed the influence of suspended matter in the solvent water to produce pure TiO_2 and stable water-based colloids at different particle concentrations and pH values. Pneumatic nebulization of TiO_2 colloids was achieved at several flow rates, and the results are discussed in terms of particle concentrations and size distributions detected in both colloidal and aerosol phases.

2. EXPERIMENTAL

2.1. Synthesis and Characterization of TiO_2 Nanoparticles

The TiO_2 nanoparticles were prepared by the microwave-assisted procedure previously reported (Gomez et al. 2012). Briefly, 30 ml of absolute ethanol (EtOH, Aldrich, St. Louis, MO, USA) were mixed with 2.0 ml of titanium tetraisopropoxide (TIPO, Aldrich, 97%) under magnetic stirring at 300 rpm. To this mixture, 3.0 ml of acetic acid (Aldrich) were added as catalyst for hydrolysis of TIPO. After stirring for 5 min, 5 ml of Milli-Q water (Millipore, Billerica, MA, USA) were added and the resulting mixture was stirred for 5 minutes. The resulting solution was transferred to a 20-ml vial and subsequently heated in a microwave oven (Milestone ETHOS 1600) at a maximum power of 400W and under rotational stirring. The oven was heated at 120°C under a heating rate of 30°C/min and kept at this temperature for 15 min. When the reaction was finished, the precipitates were separated by centrifugation and washed several times with anhydrous ethanol. The surface composition was determined by Fourier-transformed infrared spectroscopy (FTIR) in a Bruker VERTEX70. Details of the FTIR technique and results are shown in the online supplemental information (SI). The microwave synthesized TiO_2 nanoparticles ($MWTiO_2$) are compared with commercially available anatase nanoparticles purchased from Aldrich, Inc. (titanium (IV) oxide, anatase nanopowder, <25-nm particles size), herein after termed TiO_2. The crystalline state of nanomaterials was determined using X-ray diffraction (XRD) from 10° to 60° 2θ with a step size of 0.02° 2θ at 1°/s using a Rigaku D/MAX difractometer equipped with a rotor anode and a CuKα monochromatic source. The surface area and pore volume were both determined using N_2 adsorption in a Micromeritics TriStar3000 analyzer. Details on these measurements are given in the SI. Scanning electron microscopy (SEM) and energy dispersive X-ray (EDX) analysis were performed in an FEI Co. (Hillsboro, OR, USA) Inspect-F50 microscope together with an Oxford Instruments (Abingdon, UK) INCA PentaFETX3 EDX probe. Samples for SEM and EDX analysis were prepared depositing dry nanoparticles on conductive carbon tape and subsequently sputtered with Au. Transmission electron microscopy (TEM) images were recorded in a FEI F20 microscope at 200 kV accelerating voltage. The average nanoparticle size was estimated using the IMAQ Vision Builder image processing software.

2.2. Aerosol Generation and Characterization

All the aerosol generation experiments were performed at room temperature. Gas and aerosol conductions were made of graphite-lined conductive polycarbonate piping (i.d. 8 mm). Synthetic air streams for aerosol generation were dried by passing through a 150-mm column packed with silica gel and then filtered with a high-efficiency particulate air (HEPA)-cap-150 filter unit (Whatman Plc., Maidstone, UK). The jet nebulization airflow was controlled with a Bronkhorst (Ruurlo, The Netherlands) EL-FLOW mass flow controller. A scheme of the experimental is shown in Figure 1a. Nebulization of the colloidal suspensions of TiO_2 nanoparticles in Milli-Q water are performed using a polypropylene Philips SideStream® jet nebulizer. Details on the operation of nebulizer are given in the SI. The effect of nanoparticles in the formation of water droplets upon nebulization was analyzed by optical particle counter (OPC) (see below). Figure 1b shows the size distribution of filtered milli-Q water droplets obtained at different flow rates, pointing to the formation of droplets mostly under 10 μm. Moreover, Figure 1c shows that particle size distributions are similar for pure water and TiO_2 nanoparticle suspensions.

After removing the excess aerosol through an HEPA filter, the remaining stream is directed to an annular-cylindrical

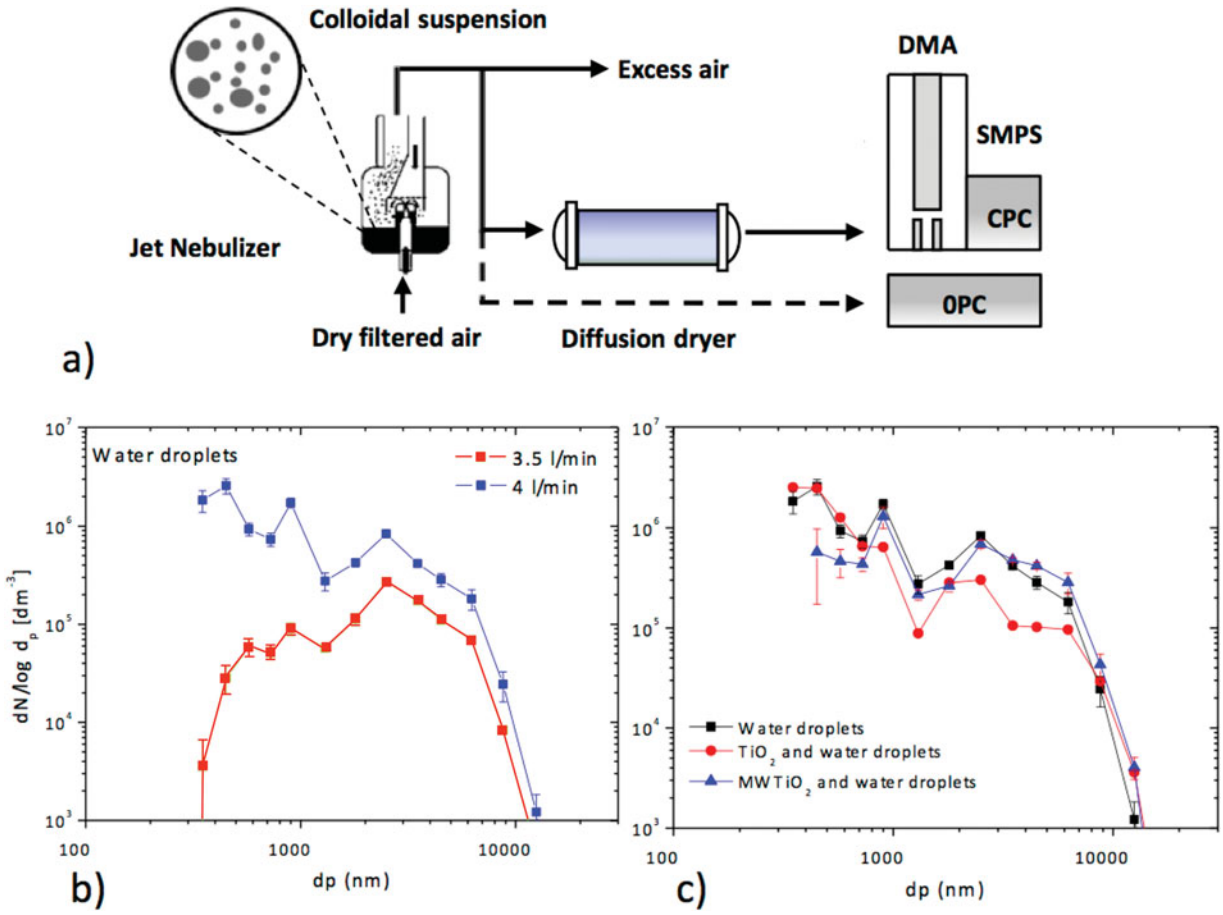

FIG. 1. Scheme of the experimental setup (a) used for nanoparticle nebulization. The system generates liquid droplets with similar sizes for both pure water (b) and nanoparticle suspensions (c). Droplet size distributions were measured using an OPC without diffusion dryer in the range from 0.3 to 20 μm. (Color figure available online.)

diffusion dryer packed with silica gel (TSI Model 3062), which is described in the SI. The adsorption of moisture drives the droplet evaporation, with a rapid formation of solid particles. Aerosol nanoparticles were neutralized by directing the gas flow to an encapsulated ^{241}Am source (3.7 MBq) and then were classified and quantified using a Grimm-Aerosol Technik, GmbH (Ainring, Germany) model #5.414 stepping mobility particle sizer (SMPS+C) formed by a Vienna-type differential mobility analyzer (DMA, Model #33–900) and a condensation particle counter (CPC). The reported number size distributions are the average of two consecutive SMPS+C scans. Results have been fitted to multimodal lognormal distribution using OriginPro 8.6 software to obtain the geometric mean diameter (GMD) and geometric standard deviation (GSD) for the different modes. To determine the fraction of aerosol particles with sizes between 300 nm and 20 μm an eight-channel OPC (OPC, Model #1.108; Grimm Aerosol Technik) was used. Finally, all exit streams were HEPA-filtered and the experimental setup was placed inside a laboratory hood equipped with HEPA filters to avoid release of aerosol nanoparticles during the experiments. Gloves and respiratory masks were worn, and the analysis area was thoroughly cleaned before and after experiments with clean room wipes and filter-equipped vacuum cleaners.

3. RESULTS AND DISCUSSION

3.1. Characterization of TiO_2 Nanopowders

The anatase structure of the TiO_2 nanoparticles was confirmed by XRD analysis, as shown in Figure 2. The diffraction peaks were positively attributed to the anatase phase of titanium oxide (JCPDS card 21–1272) and no extra peaks were detected, although rutile or brookite impurities were specifically searched for. The broadening of diffraction peaks in the XRD patterns in $MWTiO_2$ was attributed to the small particle size obtained by the microwave process. The average crystallite sizes for both materials were calculated using the Debye–Scherrer formula for the diffraction peak (101) of the anatase phase identified in the XRD patterns for both materials, giving an estimated size of 13 nm for commercial TiO_2 and about 7 nm for the $MWTiO_2$. The Brunauer-Emmet-Teller (BET) surface area of the TiO_2 was 83 m^2/g while for the $MWTiO_2$ increased

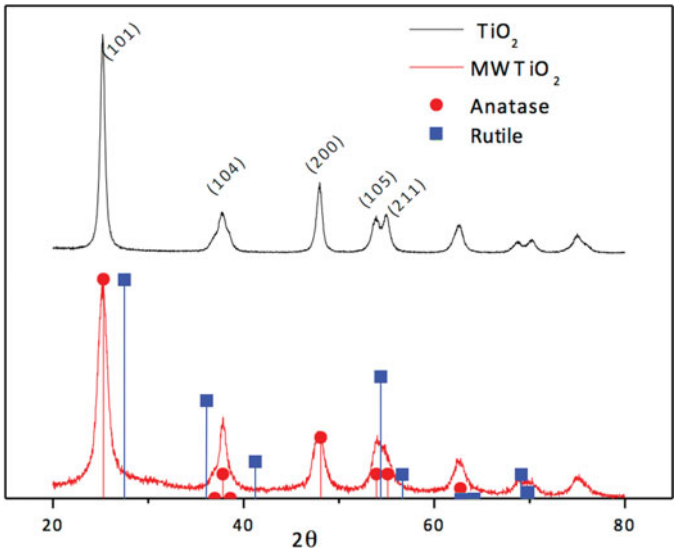

FIG. 2. XRD diffraction patterns of the TiO_2 and $MWTiO_2$ nanoparticles. Anatase and rutile peak positions are shown for identification purposes. (Color figure available online.)

up 239 m^2/g. Furthermore, the adsorption isotherms (Figure S1) indicate that the microwave synthesis gives solids with a higher pore volume and smaller pore sizes than those of the TiO_2. Also, the SEM images of commercial particles (Figure 3a) show the presence of large agglomerates, whereas in the $MWTiO_2$ images (Figure 3b) large agglomerates were not detected. The smaller crystallite sizes obtained from the XRD data indicated that the particles consisted of several smaller crystallites. These results are also in general agreement with TEM observations. For the commercial TiO_2 material (Figures 4a and b), the primary nanoparticles showed a heterogeneous distribution of shapes and sizes, forming irregular aggregates with sizes in the tens of nm range. For $MWTiO_2$, TEM images (Figures 4c and d) indicated considerable less aggregation and primary nanoparticles with prismatic shape and average size of 15 ± 4 nm ($N > 100$ particles).

3.2. Colloidal Characterization

The surface charge of TiO_2 nanoparticles changed significantly with pH due to the amphoteric character of this material (Suttiponparnit et al. 2011). In the ζ–potential versus pH plot (Figure S2), the surface charge of TiO_2 varied between 15 and -15 mV, whereas for $MWTiO_2$ the variation occurs between 27 and -33 mV, with a slightly higher isoelectric point (IEP) for TiO_2 (pH 5.8) than for $MWTiO_2$ (pH 5.4). It is interesting to note that the presence of organic residue chains grafted on the surface of $MWTiO_2$ nanoparticles, as the FTIR results show (SI), may account for the higher surface charge for these nanoparticles. The O/Ti atomic ratio determined by X-ray photoelectron spectroscopy (XPS) was 2.3 for TIO_2 and 2.5 for $MWTiO_2$, which suggests a higher surface content of oxygen for $MWTiO_2$, as could be expected, given its higher surface area, yielding a larger exposition of OH groups, which also contributed to the surface charge. The dynamic light scattering (DLS) analysis (Table 1 and Figure S3) showed that colloids of TiO_2 at any pH have larger hydrodynamic particle sizes than those prepared with $MWTiO_2$. This is in good agreement with the aggregates observed in the high-resolution TEM images of the starting material (Figure 4). In both cases, as expected, particle sizes were larger at intermediate pH values, close to the IEP (Figure S2), whereas at higher or lower pH values electrostatic repulsion decreased agglomeration.

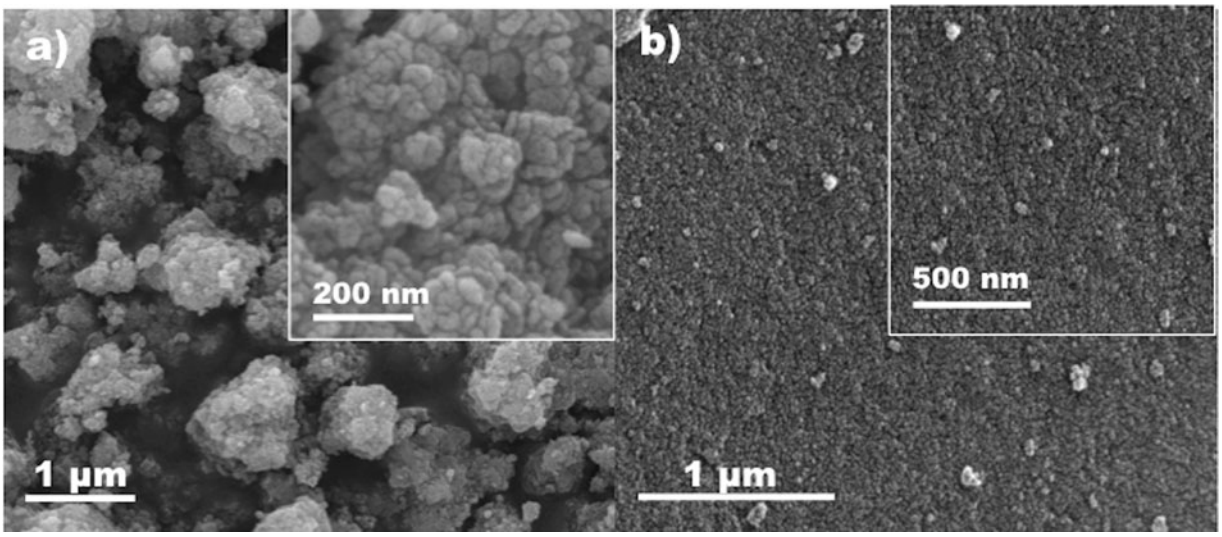

FIG. 3. SEM images of TiO_2 (a) and $MWTiO_2$ (b) nanoparticles.

TABLE 1
Particle sizes in the colloidal (measured by DLS) and in aerosol state (measured by SMPS) of TiO_2 and $MWTiO_2$ at different pH values

	$MWTiO_2$			TiO_2		
pH	D_h^a (nm)	GMD^b (nm)	GSD^c	D_h^a (nm)	GMD^b (nm)	GSD^c
11	166	34.5 106	1.73 1.63	446	59.1	1.67
5	203	14.4 80.8	1.34 1.52	803	54.6	2.08
2	195	10.1 45.6	1.25 1.49	632	37.9	1.65

[a]Hydrodynamic diameter of particles in the suspension. The polydispersity index was always under 0.2 nm; [b]geometric mean diameter of aerosol particles, determined from SMPS measurements; [c]geometric standard deviation.

3.3. Influence of Residual Particles from Water Droplets in the Nebulized Aerosols

The drying of nanoparticle-free water droplets produced in the nebulization system also generated a certain amount of residual particles (Krarnes et al. 1991). This is a common feature in droplet-based aerosol generation procedures, where the presence of impurities in the liquid leads to the formation of solids upon evaporation. Although the concentration of such water-borne impurities was usually much lower than that of the nanoparticle suspension itself, their presence could introduce significant deviations in the aerosol particle concentration and particle size distribution. These deviations became more important in relative terms as the nanoparticle concentration in the precursor suspension was reduced.

To assess and minimize the residual particle generation from the solvent, water from three different sources were used for

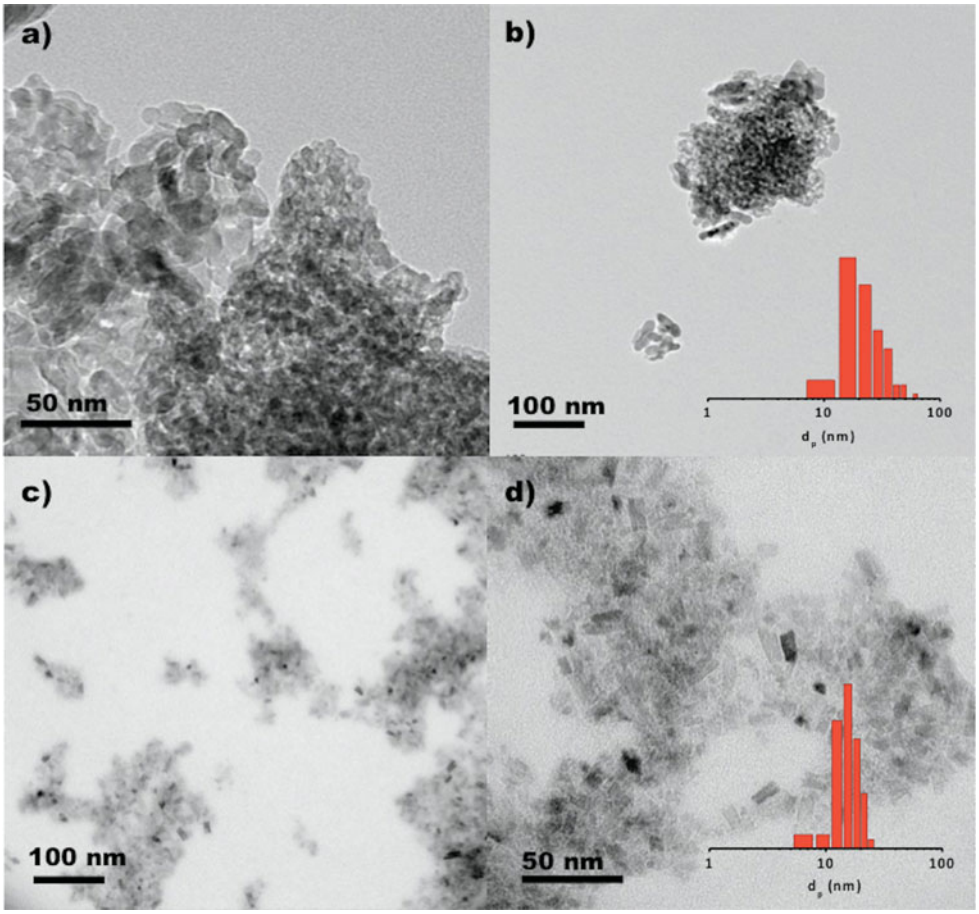

FIG. 4. TEM images of TiO_2 (a, b) and $MWTiO_2$ (c, d) nanoparticles. Insets show size histograms for both nanoparticles ($N > 100$). (Color figure available online.)

nebulization under the same conditions as for TiO_2 suspensions: (i) commercial water filtered through a 0.10-μm filter (Sigma Aldrich termed "molecular biology water," which is marketed as free of nucleases and proteases), (ii) Milli-Q water generated from Advantage A10 Water Purification Systems, that subjects the source water to filtration using a 0.22-μm filter unit and deionization to reach a resistivity value of 18.2 M$\Omega \cdot$ cm, and (iii) tap water from Zaragoza municipal water grid (conductivity value of 882 μS/cm measured at 20°C). Figure 5 shows total residual particle concentration generated by water nebulization and measured using CPC, which was notably higher for tap water (over 10^5 #/cm^3) than for the filtered "molecular biology" and "Milli-Q" varieties. The aerosol particle concentration generated from both Milli-Q and molecular biology water was similar regardless of the flow rate used for nebulization and between 10^3 and 10^4 #/cm^3, with a slightly higher aerosol particle concentration when molecular biology water was nebulized. The concentration of water-borne nanoparticle aerosol was high enough to be detected by SMPS+C; however, their size distributions show GMD values smaller than those found in aerosols obtained after the nebulization of TiO_2 and $MWTiO_2$ suspensions (Figure S6). Although residual nanoparticles were ubiquitous when generating aerosols by nebulization, their presence had little effect in the particle size distribution of aerosols obtained for nanoparticle suspensions using the same water. Taking into account these results, the nanoparticle suspensions used as aerosol precursors in the remainder of this work have been prepared using Milli-Q water.

3.4. Effect of the Air Flow Rate in the Nebulization of TiO_2 Colloidal Dispersions

Different nebulization airflows were used to generate aerosol from colloidal dispersions (1 mg/ml, pH 5) of TiO_2 and $MWTiO_2$. Figure 6 shows the number particle concentration

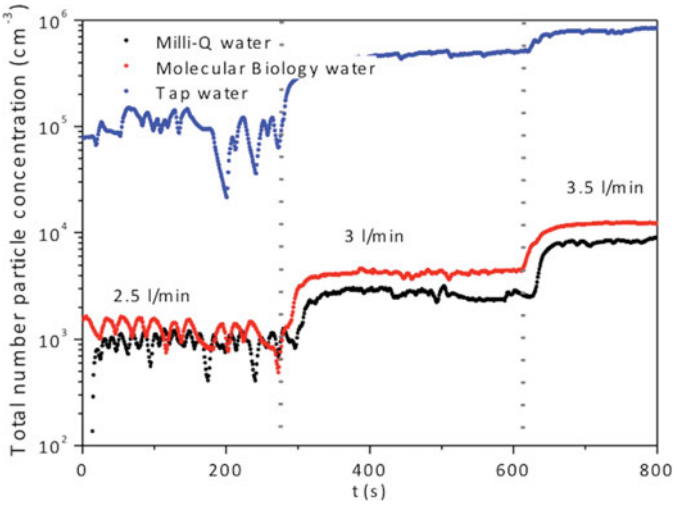

FIG. 5. Particle number total concentration (in #/cm^3) of residual particles generated upon nebulization of water of different origins as function of the flow rate. (Color figure available online.)

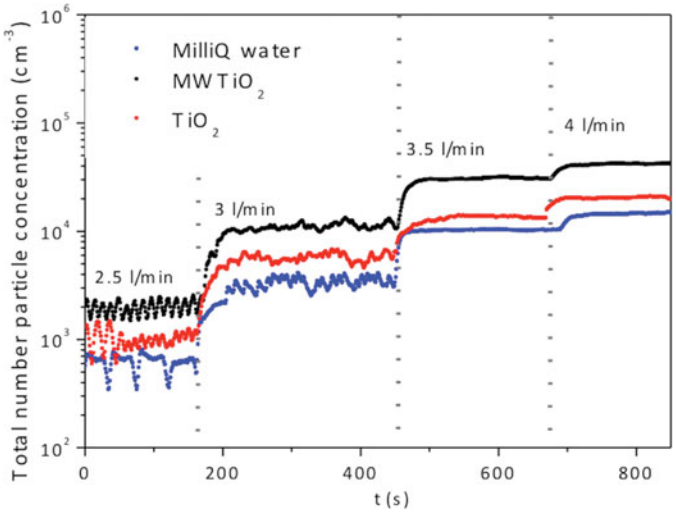

FIG. 6. Particle number total concentration (in #/cm^3) generated at different flow rates from the nebulization of colloidal dispersions (1 mg/ml, pH 5) of TiO_2 and $MWTiO_2$ nanoparticles. Particle number concentration from the nebulization of milli-Q water are shown for the sake of comparison. (Color figure available online.)

obtained with the CPC. At 2.5 l/min flow rate the number of particles generated from both colloid suspensions and from Milli-Q water is very low (under 2×10^3 #/cm^3 for TiO_2, which was the suspension giving the maximum concentrations). As the flow rate of the nebulizing air was increased, the number of droplets entrained also were risen, producing a more concentrated aerosol. This allows adjusting the concentration of the resulting aerosols, by simply changing the entraining airflow rate. Stable aerosols were obtained, with tunable concentration levels between 2×10^3 and over 4×10^4 #/cm^3. The highest concentrations were obtained with the more dispersed colloid ($MWTiO_2$) yielding up to 4.2×10^4 #/cm^3 under the conditions used in this work, while the colloid with TiO_2 reached around 2.0×10^4 #/cm^3.

Number size distributions from the generated aerosols were generally well below 200 nm for both materials at all tested airflows (Figure 7), although the TiO_2 material presented a larger fraction above 100 nm, compared with the $MWTiO_2$ nanoparticles. Only one peak with GMD of 58 nm is observed for TiO_2. On the other hand, a bimodal distribution with GMDs at 14 and 80 nm were found for the $MWTiO_2$ material. This suggested that the higher dispersion achieved in the $MWTiO_2$ suspension allowed the presence of primary particles in the aerosol. No significant changes in the GMDs of aerosol particles were found for flows ranging from 3 to 4 L/min (with a pressure drop of 210–360 mbar across the nebulizer). The number of particles generated from the more dispersed colloidal suspension of the synthesized nanoparticles reached a value around 10^4 #/cm^3, more than one order of magnitude higher than the agglomerated TiO_2, indicating the importance of achieving a high degree of colloidal dispersion in the precursor suspensions.

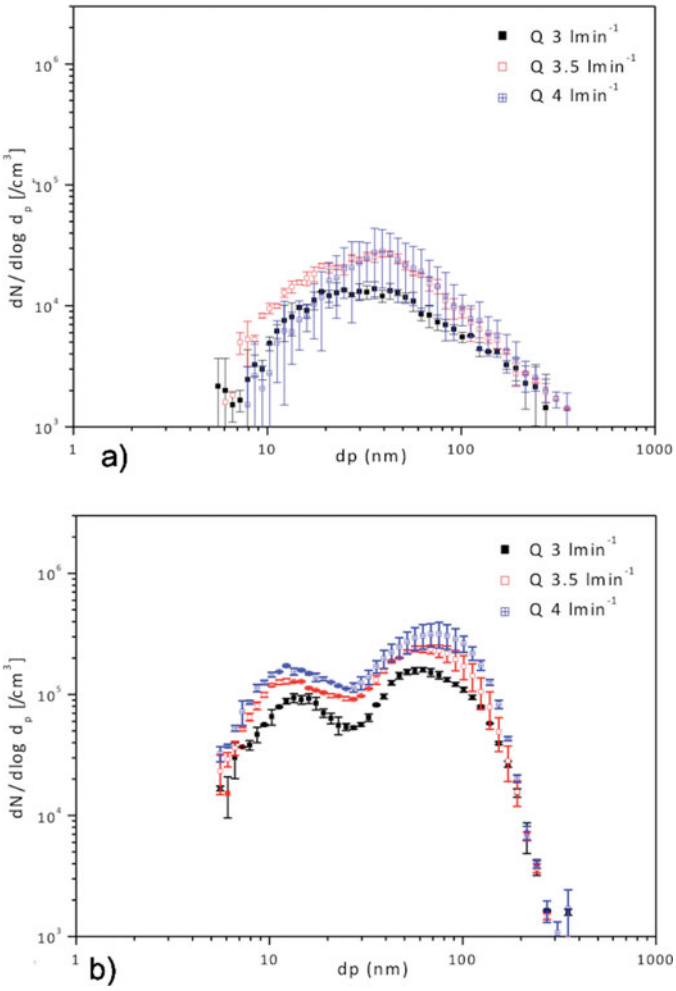

FIG. 7. Particle number size distributions (in #/cm^3) obtained at different nebulization flow rates of TiO_2 (a) and $MWTiO_2$ (b) from colloidal dispersions of 1 mg/ml at pH 5. (Color figure available online.)

Figure 8 shows the SEM images of the particles collected from the gas-phase aerosols (after liquid evaporation) using polycarbonate filter grids. The presence of pseudo-spherical aggregates with diameters mostly between 100 and 500 nm could be observed for both TiO_2 and $MWTiO_2$ aerosols, although smaller sizes were generally observed for $MWTiO_2$. The formation of such aggregates was attributed to the drying mechanism: the surface tension of the shrinking droplet maintains a spherical shape through the drying process while progressively concentrating the nanoparticles and inducing coalescence. Analogous descriptions have been previously reported for nanoparticle aerosols with similar chemical composition (Yi et al. 2004; Widiyastuti et al. 2009). Nevertheless, it has been noted that the spray drying of preformed nanoparticles may lead to diverse morphologies of the dry aggregates, depending on the drying conditions and the physicochemical properties of the dispersion (Iskandar et al. 2001; Bahadur et al. 2010). Sen et al. (2009) reported that for highly concentrated colloids the shape of the aerosol particles generated during the drying process is spherical. The self-assembly of small and well-dispersed $MWTiO_2$ nanoparticles during drying leads to highly packed spherical aggregates (Bahadur et al. 2010). Lee et al. (2009) found that generated particles morphology was highly influenced by the positive or negative surface charge of particles. Moreover, the formation of tightly packed spheres was observed for spherical silica nanoparticles (Lee et al. 2010). Although $MWTiO_2$ nanoparticles were not spherical, the homogenous size distribution would lead to the formation of highly packed spherical aggregates that could be detected in TEM images of particles collected after nebulization and evaporation (Figure S7). On the other hand, irregular agglomerates collected from TiO_2 aerosols were already present in the colloidal suspension, as it could be assessed by the large hydrodynamic diameters found in DLS analysis (Table 1 and Figure S4).

3.5. Effect of Nanoparticle Concentration in the Nebulization of TiO_2 Colloidal Dispersions

Changing the colloid concentration affected not only the initial concentration of the solids within the droplet volume but also essential characteristics of the solid suspension such as density, viscosity, and surface tension that in turn will affect the size distribution of the generated droplets and their fluid-dynamic behavior. To study the effect of the colloid concentration, suspensions of TiO_2 at 0.1 and 1 mg/ml and at pH 5 were nebulized under airflow of 3 L/min (pressure drop of 210 mbar). For both colloidal concentrations a similar GMD below 60 nm was found (Figure S6), although a small increment of GMD was in fact observed, from 33.7 nm (GSD 1.68) for 0.1 mg/ml to 54.2 nm (GSD 1.82) for 1 mg/ml. However, at higher TiO_2 concentrations the particle size distribution widened, especially toward larger sizes. This increase, as well as the observed increase in GMD, could be attributed to the formation of larger aerosol aggregate particles at high concentrations (Hinds 1999). Besides, the nanoparticle packing in the assembled grains depends on the concentration of the initial dispersion and the average packing fraction of the particles in the grain reduce with increasing concentration giving rise to large agglomerates (Bahadur et al. 2010). The so-called one-drop to one-particle mechanism is commonly accepted for describing the formation of agglomerates in aerosols (Wang et al. 2008). This model assumes that empty droplets do not lead to particles and high-particulate aerosol concentrations are reached for suspensions with high concentration, which is in agreement with the particle size distributions (Figure S5), where the more concentrated solution produced aerosols with a clearly higher concentration. Also, Shimada et al. (2009), working with NiO and C_{60} nanoparticles using a spray drying technique reported that the number concentration of droplets and, consequently aerosol nanoparticles increased with the suspension concentration, whereas the sprayed suspension volume per unit time changed little with the suspension concentration.

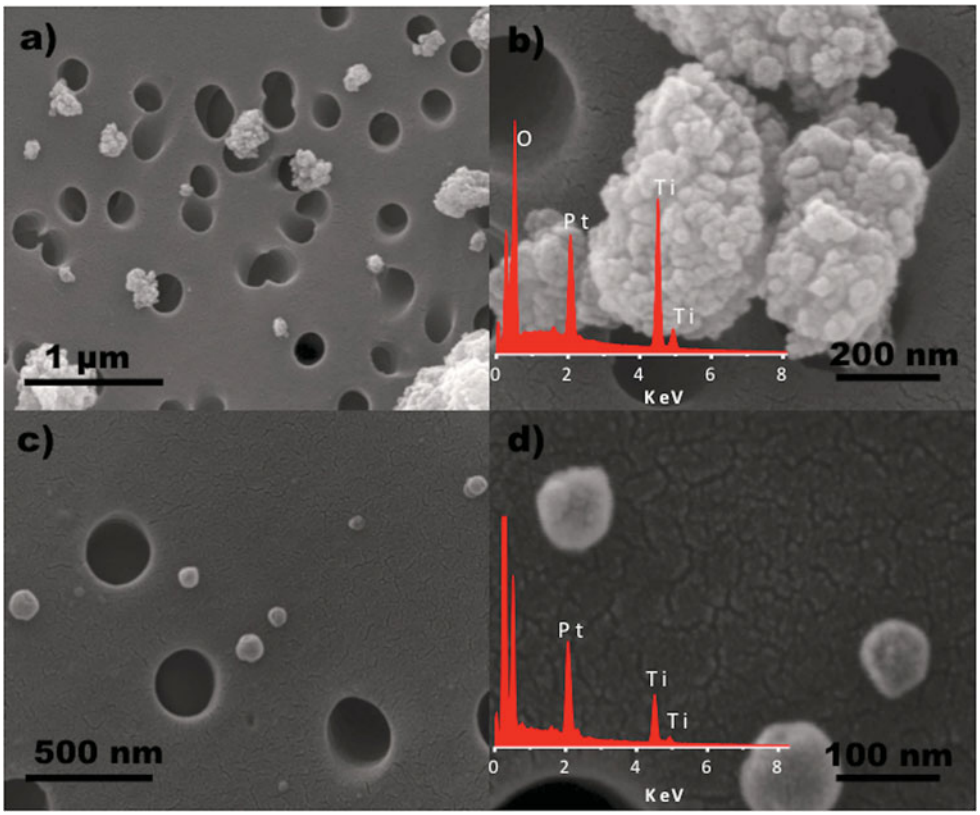

FIG. 8. SEM images of TiO_2 (a, b) and $MWTiO_2$ (c, d) nanoparticles collected on a polycarbonate filter grid at 1.2 L/min. Insets show EDX analysis. (Color figure available online.)

3.6. Effect of pH in the Nebulization of TiO_2 Colloidal Dispersions

The value of pH had a strong influence on the charge of nanoparticles in aqueous suspensions and therefore on the aggregation behavior of nanoparticles within the droplets, previous to any evaporative process. The effect of pH of colloid in the aerosol was studied with stable dispersions of 1 mg/ml of both TiO_2 and $MWTiO_2$ in water at pH 2, 5, and 11 and nebulized at 3 L/min. For both nanomaterials, aerosols with low concentrations were obtained from suspensions at pH 5, as shown in Figure 9. This pH value was close to the IEP for anatase nanoparticles, meaning that significant agglomeration was already taking place in the liquid phase prior to and during the nebulization stage (Sotto et al. 2011). Consequently, the particles were mainly present as larger-sized agglomerates leading to a lower count of aerosol nanoparticles. Some precipitation of the larger agglomerates in the nebulization vessel was observed, and the precipitated nanoparticles would not be available for aerosol formation. On the other hand, at pH 11 the ζ–potential values were around -17 and -32 mV for TiO_2 and $MWTiO_2$, respectively and stable sols are formed (Mohammadi et al. 2006), which favored both a higher content of nanoparticles in the droplets and a higher particle count in the aerosol. These results stress the importance of the colloidal particle sizes on the formation of agglomerates in the resulting aerosol. Finally, it is also worth mentioning that additional measurements using the long-range L-DMA column (for sizes 10–1000 nm) in the SMPS+C corroborate that most nanoparticles in aerosols are below 100 nm (results not shown).

Despite the differences in hydrodynamic diameters of the colloidal dispersions of TiO_2 and $MWTiO_2$ (Table 1), the average mobility diameters in the aerosol phase were similar for the case of the TiO_2 nanoparticles, where the effect of a higher pH seemed to affect the tail of the distribution toward larger particle diameters. In contrast, for the $MWTiO_2$ suspension (Figure 9) there was an increase in the GMD with pH for both peaks of the bimodal particle size distribution. According to Hernandez-Trejo et al. (2005), the sizes of the nebulized droplets depend on the design of the nebulizer system and the conditions used. Therefore, any difference in the particle size distributions can be attributed to the colloidal characteristics of TiO_2 and $MWTiO_2$ suspensions. In particular, it is worth noticing that nebulization at low pH, the lower peak of the distribution presented a sized in the range of the primary nanoparticles of the starting material (17 ± 4 nm). This suggests that the repulsive forces at this pH value (30 mV) were strong enough to maintain the individuality of a significant proportion of the nanoparticles, not only in the suspension, but also during the nebulization evaporation. The

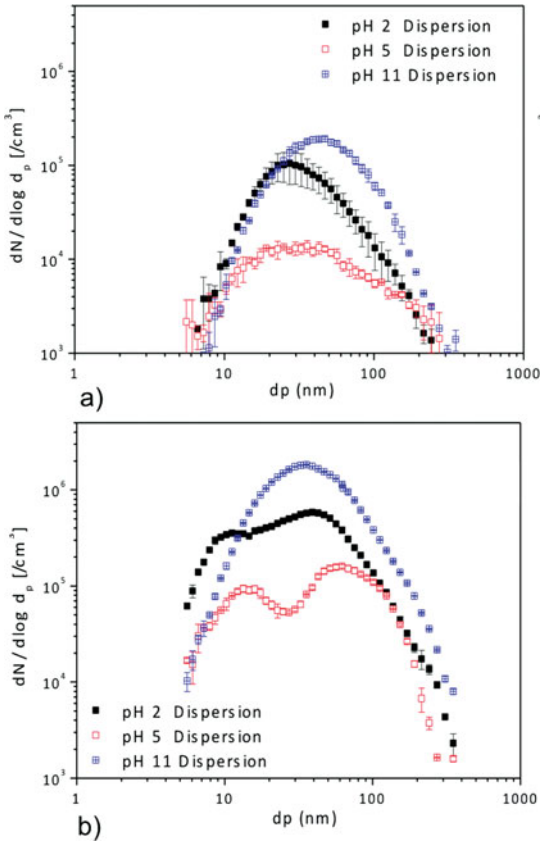

FIG. 9. Particle number size distributions (in #/cm^3) of aerosols generated from the nebulization of colloidal dispersions of TiO_2 (a) and $MWTiO_2$ (b) at different pH values. (Color figure available online.)

collection of TiO_2 and $MWTiO_2$ aerosol nanoparticles in water at different pH values led to similar particle sizes and surface charges to those observed before nebulization.

4. CONCLUSIONS

Nanoparticle aerosols with mean diameters below 100 nm are obtained after nebulization of colloidal suspensions of both prismatic 15-nm $MWTiO_2$ nanoparticles and irregular 25-nm TiO_2 nanoparticles. Small and homogeneously shaped $MWTiO_2$ leads to more uniform spheres in the aerosol, whereas the irregular TiO_2 forms a wider variety of aerosol aggregates.

Colloidal properties have a direct influence on the aerosol characteristics. The number concentration of nanoparticles in the aerosol phase is dependent on colloidal dispersion properties. When particles are not well dispersed in the colloid (e.g., when a pH close to the IEP is used), the concentration of nanoparticles in the aerosol decreases due to liquid-phase precipitation, which removes particles before droplet formation, and to aggregation that reduces the total number of particles in the aerosol while increasing the contribution of the larger nanoparticles.

REFERENCES

Bahadur, J., Sen, D., Mazumder, S., Paul, B., Khan, A., and Ghosh, G. (2010). Evaporation-Induced Self Assembly of Nanoparticles in Non-Buckling Regime: Volume Fraction Dependent Packing. *J. Coll. Int. Sci.*, 351:357–364.

Beck-Broichsitter, M., Knuedeler, M. C., Schmehl, T., and Seeger, W. (2013). Following the Concentration of Polymeric Nanoparticles During Nebulization. *Pharm Res* 30:16–24.

Borm, P. J. A. (2002). Particle Toxicology: From Coal Mining to Nanotechnology. *Inhal. Toxicol.*, 14:311–324.

Eninger, R. M., Hogan, C. J., Biswas, P., Adhikari, A., Reponen, T., and Grinshpun, S. A. (2009). Electrospray versus Nebulization for Aerosolization and Filter Testing with Bacteriophage Particles. *Aerosol Sci. Technol.*, 43:298–304.

Gomez, V., Balu, A. M., Serrano-Ruiz, J. C., Irusta, S., Dionysiou, D. D., Luque, R., et al. (2012). Microwave-Assisted Mild-Temperature Preparation of Neodymium-Doped Titania for the Improved Photodegradation of Water Contaminants. *Appl. Catal. A Gen.*, 441–442:47–53.

Henning, A., Hein, S., Schneider. M., Bur, M., and Lehr, C.-M. (2010). *Pulmonary Drug Delivery: Medicines for Inhalation Drug Delivery*. Schäfer-Korting, M. (ed), Springer, Berlin Heidelberg, 197:171–192.

Hernández-Trejo, N., Kayser, O., Steckel, H., and Müller, R. H. (2005). Characterization of Nebulized Buparvaquone Nanosuspensions—Effect of Nebulization Technology. *J. Drug Target.*, 13:499–507.

Hinds, W. C. (1999). *Aerosol Technology: Properties, Behavior, and Measurement of Airborne Particles*. Wiley, New York.

Iskandar, F., Mikrajuddin, and Okuyama, K. (2001). In Situ Production of Spherical Silica Particles Containing Self-Organized Mesopores. *Nano Lett.*, 1:231–234.

Kodas, T. T., and Hampden-Smith, M. J. (1999). *Aerosol Processing of Materials*. Wiley-VCH, New York.

Krarnes, J., Büttner, H., and Ebert, F. (1991). Submicron Particle Generation by Evaporation of Water Droplets. *J. Aerosol Sci.*, 22(Suppl. 1):S15–S18.

Lee, S. Y., Gradoń, L., Janeczko, S., Iskandar, F., and Okuyama, K. (2010). Formation of Highly Ordered Nanostructures by Drying Micrometer Colloidal Droplets. *ACS Nano.*, 4:4717–4724.

Lee, S. Y., Widiyastuti, W., Iskandar, F., Okuyama, K., and Gradoń, L. (2009). Morphology and Particle Size Distribution Controls of Droplet-to-Macroporous/Hollow Particles Formation in Spray Drying Process of Colloidal Mixtures Precursor. *Aerosol Sci. Technol.*, 43:1184–1191.

McJilton, L., Horton, C., Kittrell, C., Ogrin, D., Peng, H., Liang, F., et al.. (2009). Nebulization of Single-Walled Carbon Nanotubes for Respiratory Toxicity Studies. *Carbon*, 47:2528–2530.

Mohammadi, M. R., Cordero-Cabrera, M. C., Ghorbani, M., and Fray, D. J. (2006). Synthesis of High Surface Area Nanocrystalline Anatase-TiO_2 Powders Derived from Particulate Sol-Gel Route by Tailoring Processing Parameters. *J. Sol-Gel Sci. Technol.*, 40:15–23.

Napierska, D., Thomassen, L., Lison, D., Martens, J., and Hoet, P. (2010). The Nanosilica Hazard: Another Variable Entity. *Particle Fibre Toxicol.*, 7:39.

Noël, A., Cloutier, Y., Wilkinson, K. J., Dion, C., Hallé, S., Maghni, K., et al.. (2012). Generating Nano-Aerosols from TiO_2 (5 nm) Nanoparticles Showing Different Agglomeration States. Application to Toxicological Studies. *J. Occup. Environ. Hyg.*, 10:86–96.

Oberdörster, G., Sharp, Z., Atudorei, V., Elder, A., Gelein, R., Kreyling, W., and Cox, C. (2004). Translocation of Inhaled Ultrafine Particles to the Brain. *Inhal. Toxicol.* 16:437–445.

Oberdörster, G., Sharp, Z., Atudorei, V., Elder, A., Gelein, R., Lunts, A., Kreyling, W., and Cox, C. (2002). Extrapulmonary Translocation of Ultrafine Carbon Particles Following Whole-Body Inhalation Exposure of Rats. *J. Toxicol. Environ. Health A*, 65:1531–1543.

Park, J. Y., McMurry, P. M., and Park, K. (2012). Production of Residue-Free Nanoparticles by Atomization of Aqueous Solutions. *Aerosol Sci. Technol.*, 46:354–360.

Rossi, E., Pylkkanen, L., Koivisto, A., Nykasenoja, H., Wolff, H., Savolainen, K., et al. (2010). Inhalation Exposure to Nanosized and Fine TiO_2 Particles Inhibits Features of Allergic Asthma in a Murine Model. *Particle Fibre Toxicol*., 7:35.

Sen, D., Mazumder, S., Melo, J. S., Khan, A., Bhattyacharya, S., and D'Souza, S. F. (2009). Evaporation Driven Self-Assembly of a Colloidal Dispersion during Spray Drying: Volume Fraction Dependent Morphological Transition. *Langmuir*, 25:6690–6695.

Shimada, M., Wang, W.-N., Okuyama, K., Myojo, T., Oyabu, T., Morimoto, Y., et al. (2009). Development and Evaluation of an Aerosol Generation and Supplying System for Inhalation Experiments of Manufactured Nanoparticles. *Environ. Sci. Technol*., 43:5529–5534.

Sotto, A., Boromand, A., Zhang, R., Luis, P., Arsuaga, J. M., Kim, J., et al. (2011). Effect of Nanoparticle Aggregation at Low Concentrations of TiO_2 on the Hydrophilicity, Morphology, and Fouling Resistance of PES-TiO_2 Membranes. *J. Coll. Int. Sci*., 363:540–550.

Suttiponparnit, K., Jiang, J., Sahu, M., Suvachittanont, S., Charinpanitkul, T., and Biswas, P. (2011). Role of Surface Area, Primary Particle Size, and Crystal Phase on Titanium Dioxide Nanoparticle Dispersion Properties. *Nanoscale Res. Lett*., 6:27.

Swift, D. (1993). Aerosol Measurement in the Health Care Field, in *Aerosol Measurement Principles, Techniques and Applications*. Wiley, New York.

Verma, N. K., Crosbie-Staunton, K., Satti, A., Gallagher, S., Ryan, K. B., Doody, T., McAtamney, C., MacLoughlin, R., Galvin, P., Burke, C. S., Volkov, Y., and Gun'ko Y. K. (2013). Magnetic Core-Shell Nanoparticles for Drug Delivery by Nebulization. *J Nanotechnol*, 11:1–13.

Wang, W.-N., Purwanto, A., Lenggoro, I. W., Okuyama, K., Chang, H., and Jang, H. D. (2008). Investigation on the Correlations between Droplet and Particle Size Distribution in Ultrasonic Spray Pyrolysis. *Ind. Eng. Chem. Res*., 47:1650–1659.

Widiyastuti, W., Lee, S. Y., Iskandar, F., and Okuyama, K. (2009). Sintering Behavior of Spherical Aggregated Nanoparticles Prepared by Spraying Colloidal Precursor in a Heated Flow. *Adv. Powder Technol*., 20:318–326.

Wiesner, M. R., Lowry, G. V., Alvarez, P., Dionysiou, D., and Biswas, P. (2006). Assessing the Risks of Manufactured Nanomaterials. *Env. Sci. Technol*., 40:4336–4345.

Yeo, L. Y., Friend, J. R., McIntosh, M. P., Meeusen, E. N. T., and Morton, D. A. V. (2010). Ultrasonic Nebulization Platforms for Pulmonary Drug Delivery. *Expert Opinion on Drug Delivery*, 7:663–679.

Yi, G. R., Manoharan, V. N., Michel, E., Elsesser, M. T., Yang, S. M., and Pine, D. J. (2004). Colloidal Clusters of Silica or Polymer Microspheres. *Adv. Mater.*, 16:1204–1208.

Zhang, Y., Ali, S. F., Dervishi, E., Xu, Y., Li, Z., Casciano, D., et al. (2010). Cytotoxicity Effects of Graphene and Single-Wall Carbon Nanotubes in Neural Phaeochromocytoma-Derived PC12 Cells. *ACS Nano*., 4:3181–3186.